Energy loss in medium-energy ion scattering: A combined theoretical and experimental study of the model system Y on Si(111)

M. A. Muñoz-Márquez, G. S. Parkinson, and D. P. Woodruff*
Physics Department, University of Warwick, Coventry CV4 7AL, United Kingdom

A. Hentz and P. L. Grande
Instituto de Fisica, Universidade Federal do Rio Grande do Sul, Avenida Bento Gonçlaves 9500, 91501-970 Porto Alegre, Rio Grande do Sol, Brazil

G. Schiwietz
Abteilung SF4, Bereich Strukturforschung, Hahn-Meitner-Institut, Glienicker Strasse 100, 14109 Berlin, Germany

T. J. Wood, C. Bonet, and S. P. Tear
Physics Department, University of York, York YO10 5DD, United Kingdom

P. Bailey and T. C. Q. Noakes
CLRC Daresbury Laboratory, Daresbury, Warrington WA4 4AD, United Kingdom
(Received 20 April 2005; revised manuscript received 21 June 2005; published 11 August 2005)

The energy-loss spectrum associated with scattering of 100 keV H^+ ions from Y atoms on Si(111) has been investigated both experimentally and theoretically. Measurements were made from Y overlayers, and from the Si(111)(1×1) two-dimensional silicide phase formed by Y on this surface, in various scattering geometries and with different surface preparations. Theoretical simulations were conducted based on calculations of the energy loss experienced in specific ion trajectories through the surface, using coupled-channel calculations to describe inner-shell ionization and excitation as a function of impact parameter. The experimental results indicate that additional broadening contributions arise from surface inhomogeneity and roughness, but for near-normal incident and outgoing trajectories the theory and experiment agree quite well. The calculations show that, even for the ideal two-dimensional silicide phase in which the Y atoms lie just below the surface, significant energy loss arises from interaction of the ions with surrounding Si atoms, leading to a complete loss of intensity at zero energy loss.

DOI: 10.1103/PhysRevB.72.075415 PACS number(s): 68.49.Sf, 79.20.Rf, 61.85.+p, 34.50.Bw

I. INTRODUCTION

Medium-energy ion scattering (MEIS),[1] typically using 100 keV incident H^+ or He^+ ions, is increasingly applied to a range of problems concerned with compositional and structural characterization of the near-surface region of solids. As in conventional (MeV) Rutherford backscattering (RBS), the energy of the scattered ions is determined by the recoil energy loss, which depends on the mass of the scattering atom, and by the inelastic loss, which depends on the distance traveled by the ions through the solid. This distance of travel depends on the depth of the scatterer, so the scattered-ion energy spectrum contains information on both the depth and elemental character of atoms in the near-surface region. The lower energies used in MEIS, however, permit the use of electrostatic energy analyzers with greatly superior energy resolution to detectors used in RBS, providing far better depth resolution (of the order of single atomic layer spacings) in the composition analysis. The effect of elastic shadowing also allows one to chose incident ion directions which illuminate specific (small) numbers of near-surface layers, and through similar ("blocking") effects in the outgoing ion trajectory, to obtain quantitative information on the near-surface crystallography.

In order to extract elemental depth distributions from MEIS spectra it is usual to account for two effects which influence the shape of that part of the scattered-ion energy spectrum arising from scattering from atoms of a particular mass. One is an assumed average energy loss per unit distance traveled in the sample, typically calculated using the SRIM code.[2] In addition, however, in recognition of the fact that the energy loss is actually due to discrete electronic excitations, which are thus stochastic in nature, the scattered-ion energy peak arising from scattering from an atom at a certain depth is broadened by an amount that increases with increasing depth to account for this "straggling." Here, too, there are empirical formulas that can be applied to estimate this effect (e.g., Refs. 3 and 4). This procedure, of course, fails to take account of the details of the range of specific electronic energy-loss processes that occur and their relative probabilities; one manifestation of this is a distinct asymmetry in the scattered-ion energy spectrum from a single atomic layer which can be fitted by an asymmetric Gaussian function, but not by symmetric Gaussian or Lorentzian functions (e.g., Refs. 5 and 6). Note that in general the typical experimental energy resolution of 200–300 eV or more is sufficient to smear out the fine structure to be expected for the discrete electronic core excitations in the scattered-ion energy spectrum. Indeed, even the asymmetry becomes less

significant for scattering from deeper layers, due to the energy broadening arising from straggling, such that MEIS analysis of layers with thicknesses many times the atomic interlayer spacing can be analyzed quite effectively using only symmetric Gaussian fitting functions. It is also possible to use empirical asymmetric Gaussian functions to extract layer-dependent information from MEIS on an atomic scale,[7] yet it is clear that there would be considerable benefit in establishing a firmer physical basis for such methods.

Here we present the results of a combined theoretical and experimental investigation of the MEIS energy-loss spectrum, using 100 keV H^+ ions, from a model system, namely, Y on Si(111). This system has been chosen for several reasons. First, because the atomic mass of Y is considerably larger than that of Si, the scattered ions from Y have a much higher energy than those from Si (due to the smaller elastic recoil energy loss), and so are not superimposed in the scattered-ion energy spectrum on a background of ions scattered from the far more numerous substrate atoms. Second, Y has only a single naturally abundant isotope, so there is no energy broadening due to the presence of atoms of different masses. Third, Y has a significant number of electrons in core levels in the energy range up to 200–300 eV which may contribute to a detectable asymmetry in the scattered-ion energy spectrum. Finally, there is a structurally characterized monolayer phase of Y on Si(111), namely, a (1×1) surface silicide;[8] notice, though, that in this phase the Y atoms actually lie just below the outermost Si atomic layer, whereas an ideal experiment to probe the interaction of the ions with only a single atom would have the adsorbate atoms above the substrate. Because of this, data were also collected from low coverages of Y on Si(111), prepared under conditions which should suppress this subsurface incorporation, and may allow all Y atoms to be outside the Si substrate surface. In principle, at least, our objective was to collect MEIS scattered-ion energy spectra which involved scattering only from Y atoms, with no influence of the substrate. The theoretical calculations of the energy loss in single atom collisions are based on *ab initio* quantum-mechanical methods using full numerical atomic-orbital coupled-channel calculations.[9] In a real surface experiment the ion trajectories may also suffer energy loss through interactions with other surface atoms close to the ion trajectory, and these were included through the use of a computer program SILISH (simulation of line shape), which incorporates the results of the single-atom collision losses into a Monte Carlo calculation of the ion trajectories through the solid.

While there have been detailed measurements of ion energy-loss spectra in single atom collisions in this energy range for small-angle scattering from He atoms, together with theoretical calculations (e.g., Refs. 10 and 11), this appears to be the first such study of essentially single atom collisions from heavier atoms which also is directed to large-angle scattering (and thus small impact parameters). An exception is a similar combined theoretical and experimental study of scattering from S atoms segregated to the surface of a steel,[12] although the experimental statistics defining the asymmetric tail of the peak in this work were marginally adequate for this comparison. In addition there has been a similar comparison for 98 keV H^+ scattering from Al(110) using incident beam geometries which minimize the contributions of scattering from subsurface atoms, but inevitably involves scattering from several atomic layers of Al atoms.[13] We may also mention an earlier exploration of ways to incorporate energy loss into MEIS scattering codes, but this did not explicitly consider the details of the energy-loss processes.[14]

II. EXPERIMENTAL DETAILS AND RESULTS

The experiments were performed at the Daresbury Laboratory U.K. National MEIS facility.[15] The ion accelerator is fitted with a duoplasmatron ion source and was operated for the present studies with a H^+ beam at a nominal energy of 100 keV. The end station consists of separate ultrahigh-vacuum (UHV) chambers for sample preparation and characterization, for sample storage, and for the ion-scattering experiments. Samples are introduced into the preparation chamber via a fast-entry load lock and transferred between chambers under UHV conditions. MEIS measurements were performed with the sample at room temperature. The sample was aligned with respect to the incoming ion beam by means of a high-precision goniometer. Incident ion doses, measured by means of a tungsten mesh positioned in the beam path, were within the range typically used in other MEIS studies. The position of the beam spot on the sample surface was changed regularly to minimize ion-induced damage. Investigations of the influence of ion-induced damage revealed no significant changes in the energy spectra or blocking curves for doses between 20 and 40 μC. Ions scattered from the sample were detected by a movable toroidal electrostatic analyzer, the two-dimensional (2D) detector[16] of which provides "tiles" of ion counts as a function of both ion energy and scattering angle over limited ranges of each. Additional measurements at slightly different pass energies or angular positions allow several such tiles to be joined together to provide more extensive two-dimensional energy and angular maps as required. However, for the narrow energy range of the scattered-ion energy spectra from Y atoms which form the core of the present study only a single tile was recorded; this procedure minimizes the possible impact of errors associated with joining the 2D data tiles. The general methodology for extracting ion energy spectra and angular blocking curves from such raw data have been described elsewhere,[15,17] although for the specific objectives of the present study a specialized approach was used as described below.

In the present experiment the objective was to collect scattered-ion energy spectra from the Y atoms on, or in, the Si(111) surface, with the best possible spectral resolution and best possible statistics. To optimize the resolution the final set of slits in the ion beamline were closed down, decreasing the vertical size of the ion beam (perpendicular to the scattering plane but within the dispersion plane of the analyzer) from 0.5 to 0.15 mm. This led to a reduction of the effective ion beam current, from $\sim$60 to $\sim$20 nA, but an improvement in the overall energy resolution [full width at half maximum (FWHM)] in the measured spectra from $\sim$400 to $\sim$250 eV. Of course, the reduced beam current leads to a

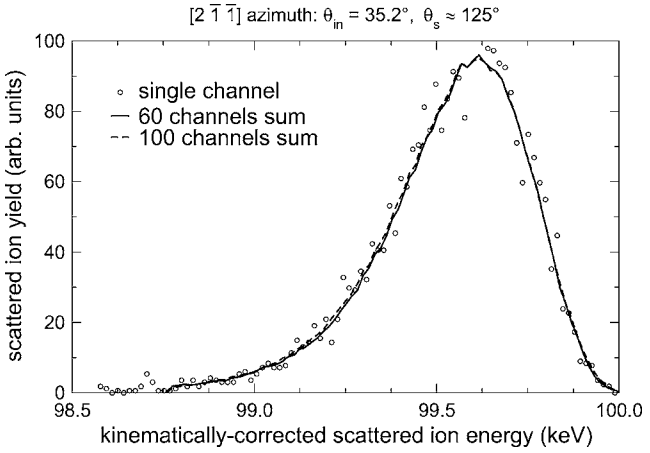

FIG. 1. Scattered-ion energy spectra, after applying the kinematical correction for the recoil energy loss, for 100 keV H^+ ions scattered from Y atoms in a 0.8 ML overlayer on Si(111), showing the effect of summing over increasing number of angular channels of the position-sensitive detector in the ion energy analyzer as described in the text.

loss of signal, and thus a deterioration in the statistical noise. To address this problem, scattered-ion energy spectra taken at slightly different scattering angles (within the 2D detector angular range) were displaced in energy by the kinematical factor (the change in recoil energy loss with scattering angle) and then summed over a finite angular range. To allow for any nonlinearities in the 2D detector[18,19] the kinematical correction factor was actually extracted from the data. To do this the shift in the Y scattering peak energy at each scattering angle within a 2D tile was determined by peak fitting, establishing a value of the kinematical factor from these individual peak energies. A smoothed version of this kinematical factor as a function of scattering angle was then used to adjust the energy scale of these scattered-ion energy spectra extracted at each scattering angle, prior to summation. Checks were made on this procedure by comparing the spectra obtained in this way for different ranges of angular integration ranging from 0.15° for a single channel of the detector to 15° corresponding to 100 such channels. Figure 1 shows such a comparison for a single channel, for 60 channels, and for 100 channels; while the spectrum obtained from the single channel contains much more statistical noise, due to the smaller number of detected ions, there is no discernible difference in the spectral peak shape. In experimental spectra shown in this paper sums are over 60 channels corresponding to an angular range of 9°. Notice that in this figure, and all later figures showing the experimental data, the energy scale is that after applying the kinematical correction factor, and so does not include the recoil energy loss of the main scattering collision. As we are concerned here only with the relative energies within the spectra that define the energy losses, this offset of the absolute energy scale is of no consequence. Indeed, small variations in the primary beam energy from experiment to experiment associated with the operating conditions of the ion source also occurred, and additional small energy shifts (typically up to ~200 eV) in the absolute energy scale have been applied to different spectra to simplify comparisons between them. The same nominal absolute energies are also used for the matching theoretical simulations described later in this paper.

The Si(111) sample was cleaned in the UHV chamber by flash annealing to 1200 °C. This procedure yielded a sharp (7×7) low-energy electron diffraction (LEED) pattern characteristic of the clean reconstructed surface, while Auger electron spectroscopy indicated no detectable impurities. The Y deposition was effected from a heated filament of tungsten, onto which Y had previously been melted, at a very low rate [~1 monolayer (ML)/h], with the pressure maintained in the 10^{-10} mbar range. Two fundamentally different surface phases were investigated. In one of these, aimed at producing a pure Y overlayer, deposition was onto the sample at room temperature and no postdeposition annealing was conducted. Two different samples were measured with Y coverages of 0.4 and 0.8 ML, as determined by MEIS. These coverages were obtained from scattered-ion energy spectra recorded using the nominal fcc one-layer double-alignment geometry of $[0\bar{1}\,\bar{1}]$ incidence and [100] outgoing ion detection. In Si the structure actually comprises double layers, so this geometry should ideally illuminate two layers, but the data were analyzed assuming this geometry actually led to a Si scattering signal equivalent to 2.2 layers, the value obtained from a VEGAS simulation[20] of this experiment from an ideally terminated (1×1) surface. Note that after Y deposition the initial (7×7) LEED pattern was lost and no clear diffraction pattern was observable, suggesting that not only the Y overlayer, but possibly the Si surface, was disordered; the true Si scattering signal may, therefore, represent rather more than these 2.2 layers. The relative Y and Si scattering signals were then corrected for their respective scattering cross sections (including a screening correction).

In the second type of surface preparation the objective was to obtain a well-ordered (1×1) surface silicide phase, but to avoid the formation of a three-dimensional silicide, characterized by a $(\sqrt{3}\times\sqrt{3})R30°$ LEED pattern. In this case a nominal 1 ML of Y was deposited onto the surface and this was then annealed to ~500 °C until a sharp (1×1) LEED pattern was seen. As no accurate method of monitoring the sample temperature was available during the annealing, the nominal temperature was estimated on the basis of a calibration based on the power input (governed by the emission current from the electron bombardment filament). Detailed measurements were made on two different preparations using slightly different annealing temperatures, referred to hereafter as the low- and high-temperature-annealed samples.

The MEIS measurements from these four distinct surface preparations, two different coverages of the overlayer, and two different annealing temperatures of the 2D silicide were made at a nominal incidence energy of the H^+ ions, in several different geometries, and for several different incidence angles (although not all scattering geometries were used for all the preparations). Two different incidence azimuths, $[2\bar{1}\,\bar{1}]$ and $[1\bar{1}0]$ (which involve different trajectories to the Y atoms in the silicide relative to the surrounding Si atoms), and two different incidence angles, 35.26° and 70.53° relative to the surface normal, were used; in the $[2\bar{1}\,\bar{1}]$ azimuth

these incident angles correspond to $[0\bar{1}\,\bar{1}]$ and $[1\bar{1}\,\bar{1}]$ directions, respectively. The average scattering angles investigated ranged from 55° to 125°.

The widths of the scattered-ion energy spectra resulting from the Y atoms are influenced by two effects, namely, the inelastic energy losses in the hard collision of the H^+ ions with the Y atom, and similar inelastic energy losses due to interaction with other (Si or Y) atoms close to the incident and scattered-ion trajectories before and after the primary hard collision. Our primary interest here is in establishing the losses associated with the single-atom hard collision, so we wish to minimize the influence of inelastic scattering due to interaction with other surface atoms. For this purpose it is reasonable to assume that the narrowest measured scattered-ion energy peaks correspond most closely to this condition. The experimental data showed the following systematic trends: (i) scattered-ion energy spectra showed narrower peaks from the 0.4 ML coverage than from 0.8 ML coverage of the unannealed Y layers, (ii) narrower peaks were seen from the lower-temperature-annealed 2D silicide phase than from the equivalent surface annealed at higher temperature, (iii) for a given incidence angle, the narrowest peaks were seen for the largest scattering angle (125°), and (iv) for this large scattering angle the peaks were narrower for 35.26° incidence than for 70.53° incidence relative to the surface normal. Typically, the variation in the widths (full width at half maximum) associated with various conditions was up to about 100 eV.

In qualitative terms, at least, all of these results can be reasonably well understood. In the case of the unannealed Y layers deposited at room temperature, one potential problem is that of Y clustering on the surface, possibly forming local 3D islands, containing subsurface Y atoms (i.e., Y atoms below other Y atoms); this effect is likely to be more serious as the coverage is increased. For the silicide layer, the wrong annealing temperature may also cause problems; too low a temperature may leave a mixture of Y atoms above the surface and Y atoms accommodated below the surface in the 2D silicide. By contrast, too high an annealing temperature may lead to some deeper subsurface incorporation associated with partial occupation of the 3D silicide phase. Scanning tunneling microscopy (STM) studies have revealed clear evidence for some surface morphology changes associated with the interaction of Y with Si(111).[21,22] Either of these effects could lead to a broadening of the scattered-ion energy peak, so while it is not obvious, *a priori*, which of our annealing temperatures would be optimal, it is reasonable that one of these temperatures would lead to a less optimally prepared sample. The results suggest it is the higher-temperature treatment which is less satisfactory, apparently leading to some deeper subsurface Y incorporation. In the case of the dependence on scattering geometry, we may expect that more grazing incident or outgoing ion trajectories will lead to greater inelastic losses to surface atoms other than the Y atom involved in the hard collision, so these effects will be minimized by a scattering geometry which has both trajectories as close as possible to the surface normal. This corresponds to the condition of 125° scattering with 35.26° incidence when the outgoing ions are detected at approximately 20° from the surface normal.

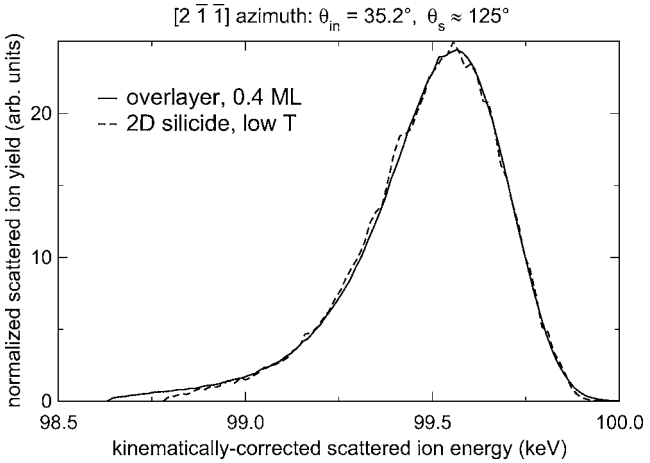

FIG. 2. Comparison of the experimental scattered-ion energy spectra from the Y atoms in a 0.4 ML overlayer and in the two-dimensional silicide phase prepared at the lower annealing temperature for 125° average scattering angle and $[0\bar{1}\,\bar{1}]$ incidence.

Our experimental results also showed that for this favored scattering geometry the scattered ion energy spectrum from Y was essentially identical for the preferred preparations of both the unannealed overlayer (0.4 ML coverage) and 2D silicide (lower temperature anneal) as shown in Fig. 2. It is therefore these experimental spectra that form the primary basis of our comparison with theoretical results, the simulations being performed for the 2D silicide phase for which the surface structure is known.[8] We should, however, note that while the trends associated with the peak broadening in the different experiments may be rationalized in a qualitative fashion, as described above, the theoretical simulations indicated that some of the observed effects cannot be reproduced quantitatively on the basis of these same arguments. These problems will be discussed more fully in the following section. As indicated above, we will continue to focus on the spectral details of the elastically backscattered 100 keV H^+ ions from the heavy Y atoms.

III. THEORETICAL DETAILS AND RESULTS

As described in the Introduction, the theoretical treatment required to compare with these experimental results requires two stages. In the first stage the details of the inelastic energy losses associated with interaction with a single scattering ion are described. These results are then incorporated into a simulation of the ion trajectories through the surface region in the experiment.

A. Inelastic excitations in single collisions

Coupled-channel calculations are the best tool to describe inner-shell ionization and excitation of atoms[9,23] as a function of the impact parameter. These time-consuming calculations are based on the semiclassical method.[24] The projectile following a classical trajectory provides a time-dependent electrostatic perturbation on the target electrons which is incorporated in a full solution of the time-dependent

Schrödinger equation. For a given impact parameter b the amplitudes $a_{i\to f}$ are calculated for any transition from an initial occupied state i to an unoccupied bound or continuum state f and thus the probability corresponding to atomic excitation or ionization is determined. Details of the atomic-orbital coupled-channel calculations may be found elsewhere.[9]

The independent-electron model is adopted for one active electron in the target atom moving in the electrostatic field due to both nuclei and the other electrons, which are included in a frozen-core Hartree-Fock-Slater framework.[25] In this way, the ground-state and excited-state wave functions (where the hole in the ith shell is not accounted for in the self-consistent potential) as well as the eigenenergies of the active electron are calculated. Since each excited or continuum state corresponds to a well-defined energy transfer $T=\varepsilon_f-\varepsilon_i$, the electronic energy-loss probability is given by

$$\frac{dP_i}{dT}(b)=\sum_f |a_{i\to f}(b)|^2\delta(T-(\varepsilon_f-\varepsilon_i)), \tag{1}$$

where the summation becomes an integral over ε_f, in the case of continuum states. Notice that for elastic collisions ($f=i$), as well as for "bound-state" excitation, the energy-loss distribution defined above contains spikes due to the discrete atomic level structure. Broadening effects originating from state lifetime, bandwidth, and the Doppler effect are not considered explicitly since they are much smaller than the experimental resolution. In the framework of the independent-electron model, the probability for a certain total electronic energy loss ΔE transferred during an individual ion-atom collision can be written as

$$\frac{dP^{elec}_{atom}}{d\Delta E}(b)=\left(\prod_i \int dT_i \frac{dP_i}{dT_i}(b)\right)\delta\left(\Delta E-\sum_i T_i\right), \tag{2}$$

where the index i runs over all electrons for each subshell ($2s$, $2p$, $3s$, and $3p$ of the Si atom and $3s$, $3p$, $3d$, $4s$, $4p$, $4d$, and $5s$ of the Y atom). Here the Si K shell and Y K and L shells have not been taken into account since they are kinematically suppressed for protons at 100 keV. Equation (2) corresponds to a series of convolutions of individual single-electron energy-loss distributions and thus the whole distribution is unitary.

Figure 3 shows the results of the coupled-channel calculations for the energy-loss probability of 100 keV H^+ projectiles colliding with atomic Y at an impact parameter b close to zero. This and subsequent figures showing the theoretical energy-loss probabilities are plotted using a decreasing energy loss on the abscissa to simplify comparison with the experimental scattered-ion energy spectra. Here we have treated the projectile motion as a straight line to the apsis and the protons are penetrating the maximum electronic density (the reliability of this approximation is discussed below). The elastic peak (the peak at $\Delta E=0$) is not shown here because of the problems of representing this intense feature of infinitesimal width. A notable aspect of the energy-loss distribution in Fig. 3 is the significant contribution of excitation of Y inner subshells ($n=3$) at large energy transfers. These peaks correspond to the onset of single, double, and triple Y ionization (the corresponding subshells are indicated in the figure). However, these peaks are smeared out if one includes the effect of an experimental resolution of about 200 eV. We stress that in contrast to approaches based on perturbation theory, all results from the coupled-channel method are unitary (occupation probabilities sum up to 1 for each active electron). This unitary behavior leads to a reduction of the elastic scattering intensity when inelastic channels are important. In the present case, backscattering is almost always accompanied by excitation or ionization events, involving mainly inner-shell electrons. This is the reason for high backscattering yields at nonzero energies in the figure.

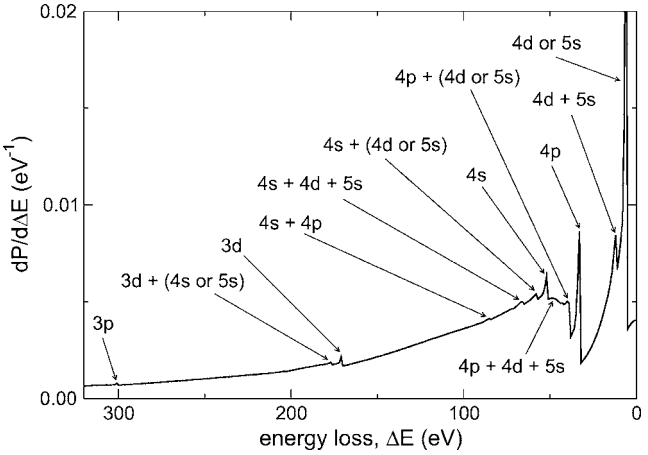

FIG. 3. Calculated results for the energy-loss probability for a single collision with an impact parameter close to zero for H^+ ions impinging on an isolated Y atom. Note that in this and subsequent theory figures the abscissa is shown with the energy loss increasing from right to left to simplify visual comparison with the experimental scattered-ion energy spectra.

For large backscattering angles, one might question the use of straight-line trajectories for the projectile motion, but calculations using curved trajectories show very little difference in the calculated energy-loss spectrum, as may be seen in Fig. 4. The curve labeled "dynamic-curved," corresponding to a scattering angle of 90°, was calculated using classical projectile trajectories that are influenced by the target nucleus as well as by the dynamic electron density of the active electron. The other curves have been determined by using straight-line trajectories. These results also show that there is very little variation in the energy-loss spectrum over a range of impact parameters corresponding to scattering angles from 5° to 125°. In order to allow a more direct estimate of the (small) probability of pure elastic scattering relative to scattering events which also involve inelastic scattering, the elastic peak (at $\Delta E=0$) is included in Fig. 4 by convoluting it with a narrow Gaussian distribution chosen to be sufficiently wide to allow reasonable visual estimate of the underlying area in the figure (standard deviation 3 eV corresponding to a FWHM of approximately 7 eV). This same small degree of broadening of the no-loss peak has also been included in the remainder of the theoretical spectra presented here.

While Figs. 3 and 4 provide information on the energy losses associated with the primary hard collision with a Y

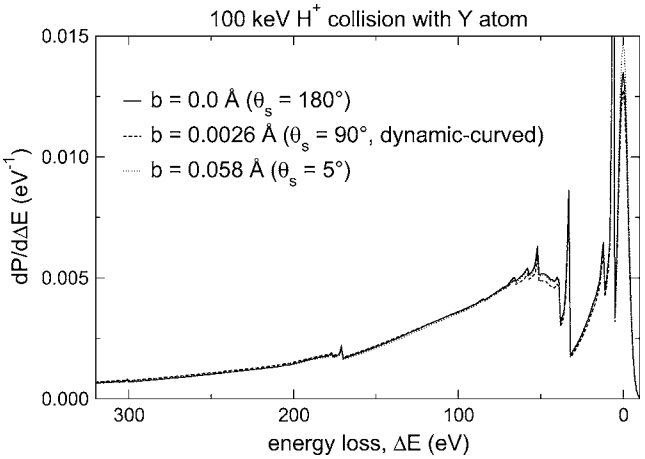

FIG. 4. Calculated results for the energy-loss distribution for H^+ ions impinging on an isolated Y atom for different impact parameters (and associated scattering angles) using dynamic-curved and straight-line projectile trajectories. The no-loss features in the theoretical spectra have been convoluted with a narrow Gaussian (FWHM approximately 7 eV) in order to broaden them sufficiently to allow their inclusion in the plots.

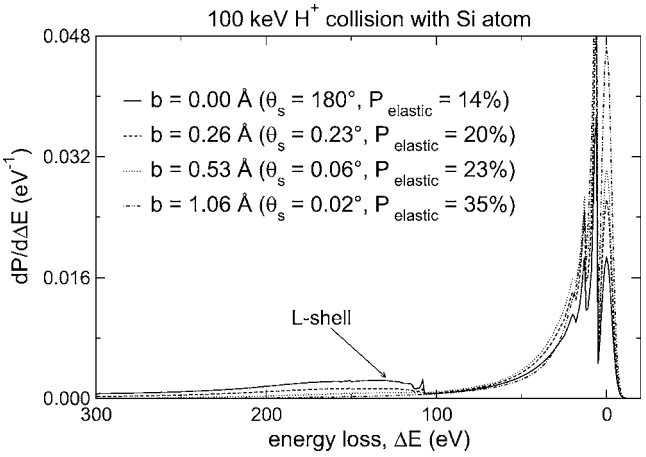

FIG. 6. Calculated results for the energy-loss distribution for H^+ ions impinging on an isolated Si atom for different impact parameters. The no-loss features in the theoretical spectra have been convoluted with a narrow Gaussian (FWHM approximately 7 eV) in order to broaden them sufficiently to allow their inclusion in the plots.

atom in our experiments, the ion trajectories in such an experiment also pass sufficiently close to other atoms to allow inelastic losses, even though the associated elastic scattering angle may be negligibly small. Figure 5 shows the energy-loss distributions for the larger impact parameters associated with such interaction, calculated using straight-line projectile trajectories. The corresponding values of the scattering angle θ, determined by the two-body interaction between the projectile and screened nucleus, are also indicated for $\theta > 0.01°$. The no-loss peak is not shown in these spectra, but its area $P_{elastic}$ is indicated for each curve. For example, for collisions with impact parameters smaller than the amplitude of typical thermal vibrations (about 0.1 Å), the probability of pure elastic (no-loss) interaction is only about 10%. Even at an impact parameter of 1.59 Å, more than half of a typical interatomic spacing in a solid, the integrated loss probability is 45%. Inspection of these figures shows that the probability of any particular energy loss only changes significantly if the impact parameter b exceeds the associated shell radius (about 0.2 Å for 3*d* and 0.75 Å for 4*s* and 4*p* orbitals). At such large values of b, the scattering angles are extremely small.

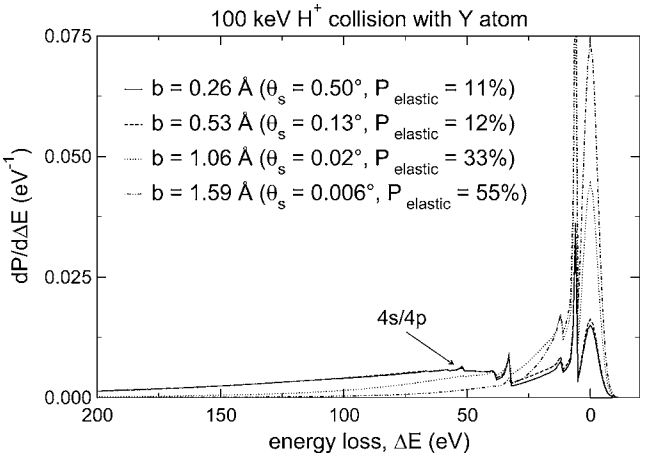

FIG. 5. Calculated results for the energy-loss distribution for H^+ ions impinging on an isolated Y atom as in Fig. 4, but for a different range of impact parameters. The no-loss features in the theoretical spectra have been convoluted with a narrow Gaussian (FWHM approximately 7 eV) in order to broaden them sufficiently to allow their inclusion in the plots.

This situation is quite general and is equally true for interactions with Si atoms present in the silicide. Figure 6 shows the impact-parameter dependence of the energy-loss distributions in collisions with an isolated Si atom. Only for collisions with impact parameters larger than the Si *L* shell (about 0.25 Å) does the energy-loss spectrum change substantially. In our experiments on the 2D Y silicide, the incident protons pass close to a Si atom before undergoing the small-impact-parameter scattering from an Y atom, and thermal vibrations increase the probability that the proton may excite or ionize the Si atom at somewhat smaller impact parameters before hitting the Y atom. Similar effects occur for the outgoing path, and together these interactions enhance the energy loss, and thus broaden the scattered-ion energy spectra detected in our MEIS experiments, as will be shown in the next section.

As a more direct indication of how the various energy-loss probabilities scale with impact parameter, Fig. 7 shows the probability of removing electrons from a few specific shells in Y and Si atoms as a function of impact parameter. This figure shows very directly the way the excitation probability falls off when the impact parameter exceeds the shell radius.

B. Monte Carlo simulations of MEIS energy-loss spectra

In order to calculate the energy-loss spectra relevant to the real MEIS experiment for the 2D Y silicide on Si(111) one

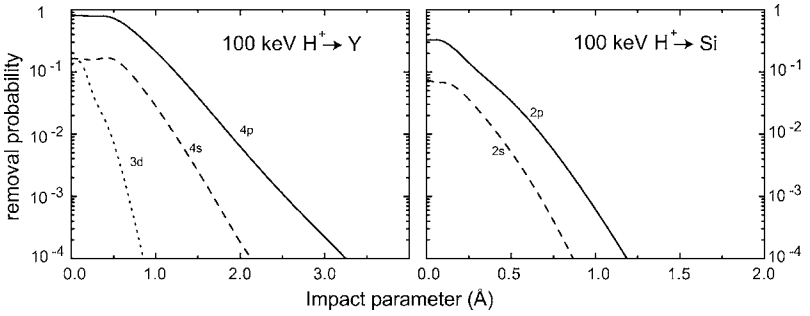

FIG. 7. Results of theoretical calculations of the probability of removing electrons from specific shells as a function of impact parameter in Y and Si atoms due to 100 keV H^+ scattering.

must consider the interactions along the scattered-ion trajectories using the SILISH code referred to in the Introduction. Briefly, to achieve this, as in the VEGAS program,[20] the lattice positions of the Y and Si atoms are stored in an array. For each impinging projectile the target atoms are displaced according to their one-dimensional root-mean-square thermal vibrations, and the ion trajectory is determined by a sequence of binary collisions. In each of them, the scattering angle is obtained by using the Molière scattering potential, the ion energy, and the impact parameter. The scattering angle is used to determine the new ion direction as well as the recoil-energy transfer to the target atom. This impact parameter is also used to select the associated inelastic energy loss tabulated from calculations based on Eq. (2) (as depicted in Figs. 3–6) for different targets and impact parameters. The target atoms are selected by considering the atoms inside a cylinder with radius r_{max} and axis parallel to the ion incident direction.

The flux of incident ions at each lattice position is then stored in a 2D matrix, where each bin, representing the transverse ion position, contains not only the number of projectiles, but also the histogram of ion directions and energy losses. The same calculation is performed for the outgoing ions in the detection direction using time reversibility. The incoming and outgoing tracks are connected by using the corresponding flux matrices, together with the position of the backscattering atom according to its thermal vibration. Only trajectories having the same scattering plane are connected. The corresponding energy loss for the whole ion trajectory therefore consists of the energy loss due to the incoming and outgoing paths, as well as to the elastic and inelastic energy loss in the hard scattering collision. In this way, the variation of the kinematical factor due to different scattering angles is also taken into account. While quite large values of the cylinder radius r_{max} ($\sim$4 Å) are needed to fully converge the calculation, some improvement in computational speed was achieved without significant loss of precision by using a somewhat smaller value ($\sim$2 Å) and including a correction to the final energy-loss spectrum. Moreover, this method of calculation avoids double counting of energy losses from more distant atoms which may fall into both the ingoing and outgoing trajectory cylinders if these cylinders are too large.

An important initial result of the application of these calculations to the Si(111)/Y system is that for the (1×1) surface silicide phase, even in the geometry with near-normal incidence and detection (35.2° incidence, 125° scattering angle) the proximity of the ion trajectory to the surface Si atoms leads to significantly more energy loss than that seen in scattering from a single Y atom with electronic energy losses only involving this Y atom. Figure 8 shows the results of these two calculations. As in Fig. 4, the single collision shows a significant peak at or near the no-loss energy which is clearly distinct from the broad loss structure. By contrast, the same scattering event from the Y atom in the surface silicide, in which the ions pass close to surface Si atoms, shows no significant intensity at the no-loss energy, while the overall spectral weight of the whole peak is displaced somewhat to higher energy loss. Even with perfect experimental energy resolution, therefore, Fig. 8 shows clearly that much of the detail of the single-atom energy loss spectrum is lost due to the interaction with nearby surface Si atoms, and particularly Si $2p$ excitations.

IV. EXPERIMENT-THEORY COMPARISON AND DISCUSSION

In comparing the experimental results with those of the theoretical simulations we may investigate two general features; one is the most obvious one of whether the narrowest experimental line shape agrees with that predicted theoretically after taking account of the experimental resolution. The second is whether other aspects of the measurements, such as the change in linewidth of the scattered-ion energy spectrum

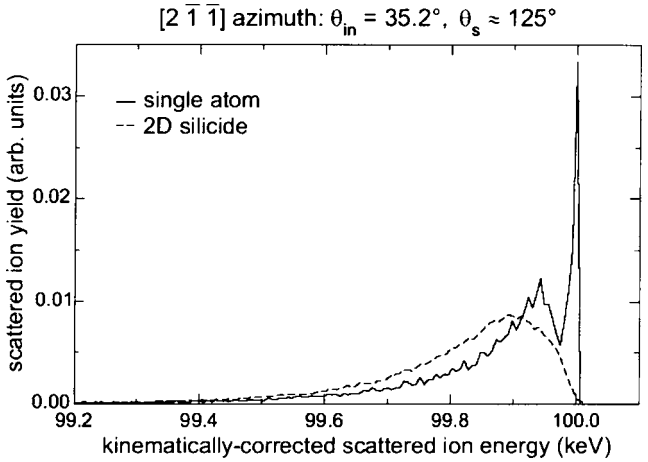

FIG. 8. Theoretical calculations of scattered-ion energy spectrum for scattering from an isolated Y atom and the same Y atom in the Si(111)(1×1)-Y surface silicide phase with an incidence angle of 35.2° and a scattering angle of 125°. Both calculations were performed using the SILISH computer code which follows a finite number of ion trajectories and thus leads to some statistical noise.

from the Y atoms with scattering geometry, are reproduced by the theory.

Before any such comparisons can be conducted, however, the theoretical energy-loss spectra must be convoluted with the experimental instrument function. This is a nontrivial problem because this function, defining the instrumental contribution to the line shape, is unknown, and indeed one might typically try to extract this from a measurement of the scattered-ion energy spectrum from a target which introduces the least possible intrinsic broadening. Unfortunately, such a spectrum corresponds to a measurement of scattering from a single isolated atom—precisely the experiment we have tried to conduct as a means of studying the intrinsic broadening. We have attempted to determine the instrument function by sending the ion beam directly into the analyzer, although to prevent damage to the detector from the high flux this was done with all lenses in the ion beam transfer system turned off, and with a very small (0.05 mm) final vertical slit, producing a low-intensity and highly collimated beam. This yielded a symmetric peak with a FWHM of 160 eV for 100 keV incident ions. However, this probably only defines a lower limit to the instrument function in a scattering experiment, as there will be additional broadening due to the larger beam size and the angular divergence of the scattered beam, the magnitude of which is unknown. In order to address this problem in the treatment of our Y scattering spectra we have explored a range of different possible instrument functions, comparing the experimental spectrum from the surface silicide measured in the favored geometry (35.2° incidence, 125° scattering angle) with the theoretical spectrum broadened by the test instrument function. Our starting point is that the instrument function should be symmetric; while it is certainly possible to imagine instrumental effects which could lead to some asymmetry, this seems to be an important initial constraint if our main purpose is to investigate the asymmetry introduced by the inelastic energy losses. The simplest assumption would be a Gaussian function, but one could also imagine a function more rectangular in form might be appropriate, as this would result from finite apertures in the ion energy analyser but infinitesimal source size and divergence. A general function for the intensity and a function of energy E of this type is $I=I_0 \times \exp\{-[\ln(2)/2]|E/\mathcal{F}|^w\}$ where $\mathcal{F}$ is the FWHM; in the special case that $w=2.0$ this becomes a Gaussian function. Because we expect the true (unbroadened) energy-loss spectrum to have a sharp cutoff at zero energy loss, we have adjusted the FWHM and w value of this instrument function to fit the high-energy side of the experimental scattered-ion energy spectrum; the quality of the fit between experiment and theory on the low-kinetic-energy (higher-energy-loss) side of the peak then defines the extent to which our theoretical calculation of the energy-loss spectrum provide a good description of the experimentally observed peak asymmetry. Notice that this assumption that the high-kinetic-energy side of the experimental ion energy spectrum is dominated by the instrumental function actually depends on the relative intensity of the no-loss feature in the energy-loss spectrum. If the energy-loss spectrum is dominated (in terms of peak area) by the no-loss feature, this assumption is valid. On the other hand, if this no-loss peak is only modest in size relative to the loss structure beyond the Y 4*s*-4*p* or Si 2*s*-2*p* thresholds (e.g., Figs. 5 and 6 with small impact parameters), this assumption is likely to be inappropriate. In fact, according to our unbroadened calculations for Y scattering in the surface silicide phase (Fig. 8) there is actually essentially *zero* intensity in the no-loss peak, but the result is a broad asymmetric function with the high-energy cutoff much sharper than the low-energy tail. In this case our assumption again becomes valid. Figure 8 also shows the comparable spectrum for an isolated Y atom, but using the same SILISH computer code which, by following a finite number of ion trajectories, leads to statistical loss of information in the energy spectrum relative to those shown in Figs. 4–6.

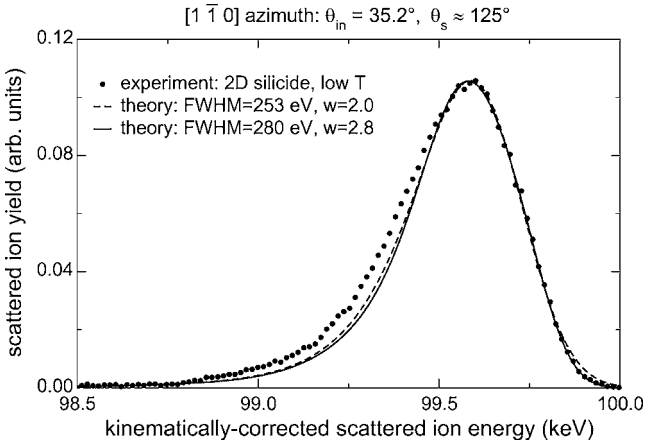

FIG. 9. Comparison of the silicide energy spectrum of Fig. 2 with the corresponding theory including the optimum broadening and the optimum Gaussian broadening.

Figure 9 shows a comparison of the experimental MEIS spectrum recorded from the low-temperature preparation of the 2D silicide in the $[0\bar{1}\,\bar{1}]$ incidence direction with an average 125° scattering angle (Fig. 2) and the theoretical simulation of this same scattering experiment, using two different instrument functions. The best-fit instrument function to the high-energy side of the experimental spectrum has a FWHM of 280 eV with $w=2.79$, but Fig. 9 also shows that a Gaussian function ($w=2.00$) with a FWHM of 253 eV gives only a marginally worse fit. This figure thus represents our best estimate of the quality of the overall experiment-theory comparison. Clearly the overall fit is not perfect: the experimental spectrum shows significantly more intensity in the intermediate energy-loss range around 300 eV below the peak. There are two possible reasons for this discrepancy. One possibility is that the theory underestimates the strength of these energy losses, but the other is that the experimental spectrum does not represent scattering only from Y atoms in an ideal Si(111)(1×1)-Y surface silicide phase. In this regard, there are several aspects of the experimental results which indicate that at least part of the discrepancy is due to this second problem. One is the fact that the spectral width of the experimental measurements from the two different preparations of the Y overlayer and the silicide differed. Figure 10 shows the spectra from the two different preparations of the unannealed Y overlayer in the geometry of the silicide measurements of Fig. 9 (35.2° incidence, 125° scattering angle).

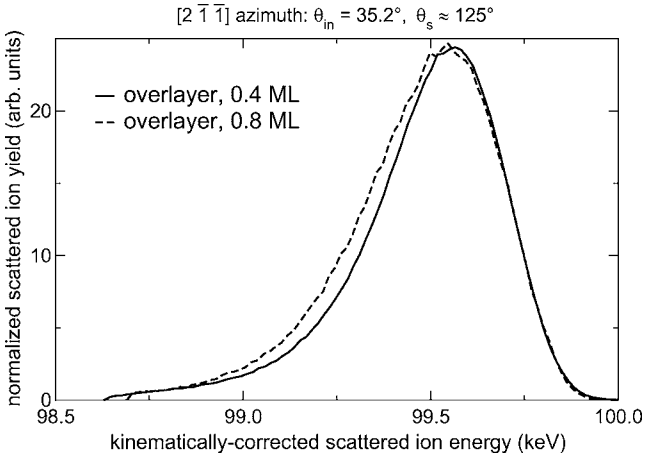

FIG. 10. Comparison of experimental scattered-ion energy spectra from the two different preparations of the Y overlayer phase on Si(111).

The increased width for the higher dose can only be attributed to clustering or partial subsurface penetration, but this leaves open the question of whether this same effect also contributes to the width of the narrower spectrum.

The same effect is seen in the measurements from the two different preparations of the 2D silicide phase, as seen in Fig. 11. Three experimental spectra are shown in this figure, all involving 125° scattering angle, but only one (the same spectrum as in Fig. 9) with the incidence angle of 35.2°. This spectrum was recorded from the silicide formed with lower-temperature annealing, but unfortunately this geometry was not used in a measurement from the sample subjected to a higher-temperature anneal. However, spectra from both preparations are seen using an incidence angle of 70.5°, and there is a clear difference in spectral width; here, too, we must assume the wider spectrum involves a less ideal sample, but cannot be sure that the narrower spectrum corresponds to an ideal surface. Figure 11 also shows the very pronounced increase in spectral width seen between the two different scattering geometries from the same sample. In

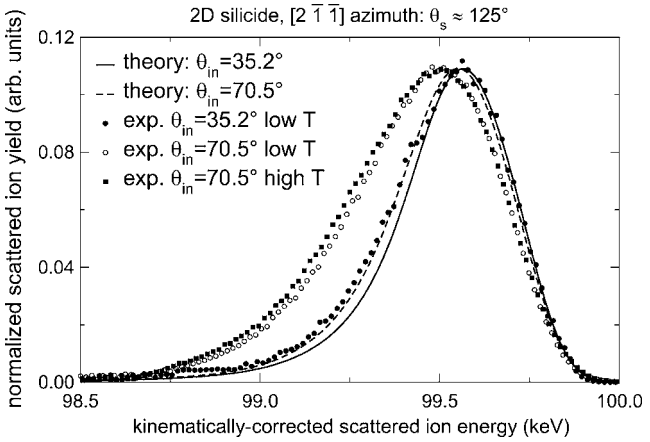

FIG. 11. Comparison of some experimental scattered-ion energy spectra from the two different preparations of the 2D surface silicide phase of Y on Si(111), together with simulations of the effect of different scattering geometries from an ideal 2D surface silicide.

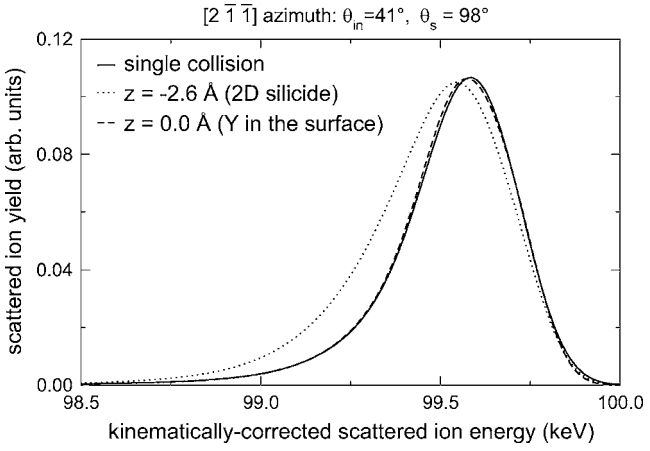

FIG. 12. Theoretical simulations (including instrumental broadening) of the scattered-ion energy spectra from scattering from an isolated Y atom and from Y atoms at different heights above a Si(111) surface.

part, at least, this can be attributed to the fact that using an incidence angle of 70.5° the incident trajectory passes much closer to the surface, allowing enhanced energy loss due to interaction with other atoms close to the ion trajectory. Qualitatively, this effect is predicted by the calculations for an ideal 2D silicide, as seen by the two curves in Fig. 11, but the magnitude of the effect seen in these theoretical calculations is much smaller than that seen in the experimental spectra.

Of course, one might argue that this effect of enhanced energy loss in the more grazing ion trajectories is also due to an underestimate of the magnitude of the effect in the theory. On the other hand, Fig. 12 shows that the theory predicts a very significant enhancement of the energy loss intensity, and thus of the spectral width, when an Y atom is moved from a site coplanar with the Si surface layer (for which the spectrum is almost identical to that of an isolated Y atom, and hence to any height above the surface), to below the surface as in the 2D silicide. By contrast, Fig. 2 shows that the narrowest spectral peaks recorded from the overlayer and silicide phases experimentally are almost identical. Clearly the theory cannot both underestimate and overestimate the strength of the inelastic scattering in essentially the same calculations, so while we cannot exclude a contribution to the theory-experiment discrepancy due to inadequacies of the theoretical calculations, there is clear evidence that a significant contribution to this discrepancy arises from the fact that the surfaces fall short of the ideal structures used in the simulations.

In fact previous work to characterize the behavior of Y on Si(111) using STM,[21,22] a method which allows one to gain some insight into the surface inhomogeneity and changes in surface morphology, certainly does indicate that either with or without annealing the surfaces are far from perfect. We have already mentioned the possible influence of clustering on the surface (especially for the unannealed surface preparations) and subsurface incorporation (especially for the annealed surfaces), both of which will lead to some of the Y atoms lying deeper below the surface than expected, and thus

to enhanced inelastic energy loss. Both of these effects would also lead to a stronger enhancement of the energy losses with ion trajectories, either ingoing or outgoing, which are more nearly grazing to the surface. Attempts to improve the agreement with the energy-loss spectra by assuming partial occupation of the 3D silicide did not prove successful, because the calculations indicated significant blocking, but this conclusion is sensitive to the exact structure of this phase. Possibly most important, however, is the increase in atomic-scale roughness, such as step creation, which has been reported in STM studies; this will also lead to enhanced loss intensity for more grazing trajectories, even if the 2D silicide or unannealed overlayer is *locally* ideal.

V. CONCLUSIONS

The results of our calculations of ion energy loss in MEIS due to electronic excitations provide insight into the role of both the primary scattering atom and other near-surface atoms in determining the spectral line shape of scattered-ion energy spectra from near-surface species. Comparison of the narrowest experimental line shape observed for Y on Si(111) using near-normal incidence and detection show generally good agreement but indicate some enhancement of the overall intensity of the energy-loss component. Evaluation of the more complete experimental data and previous work on the characterization of the Si(111)/Y surface phases suggest that problems in surface roughness and inhomogeneity are probably the main source of this discrepancy. In this regard, it would be interesting to perform similar studies of another overlayer system in which clustering and subsurface incorporation are known to be less significant.

ACKNOWLEDGMENTS

The authors acknowledge funding support by the Engineering and Physical Sciences Research Council (U.K.), by CNPq and CAPES (Brazil), and by DAAD within the PROBRAL contract (Germany).

*Corresponding author.
Electronic address: d.p.woodruff@warwick.ac.uk

[1] J. F. van der Veen, Surf. Sci. Rep. **5**, 199 (1985).
[2] J. F. Ziegler, Computer code SRIM code, http://www.SRIM.org
[3] W. K. Chu, Phys. Rev. A **13**, 2057 (1976).
[4] Q. Yang, D. J. O'Connor, and Z. Wang, Nucl. Instrum. Methods Phys. Res. B **61**, 149 (1991).
[5] D. P. Woodruff, M. A. Muñoz-Márquez, and R. E. Tanner, Curr. Appl. Phys. **3**, 19 (2003).
[6] Y. Kido, S. Semba, and Y. Hoshino, Nucl. Instrum. Methods Phys. Res. B **219–220**, 599 (2004).
[7] M. A. Muñoz-Márquez, G. Parkinson, P. D. Quinn, M. Gladys, R. E. Tanner, D. P. Woodruff, T. C. Q. Noakes, and P. Bailey Surf. Sci. **582**, 97 (2005).
[8] C. Rogero, C. Polop, L. Magaud, J. L. Sacedón, P. L. de Andrés, and J. A. Martín-Gago, Phys. Rev. B **66**, 235421 (2002).
[9] G. Schiwietz, Phys. Rev. A **42**, 296 (1990); P. L. Grande and G. Schiwietz, *ibid.* **44**, 2984 (1991); G. Schiwietz and P. L. Grande, Nucl. Instrum. Methods Phys. Res. B **69**, 10 (1992); P. L. Grande and G. Schiwietz, Phys. Rev. A **47**, 1119 (1993).
[10] T. J. Kvale, D. G. Seely, D. M. Blankenship, E. Redd, T. J. Gay, M. Kimura, E. Rille, J. L. Peacher, and J. T. Park, Phys. Rev. A **32**, 1369 (1985).
[11] G. Schiwietz, P. L. Grande, C. Auth, H. Winter, and A. Salin, Phys. Rev. Lett. **72**, 2159 (1994).
[12] W. H. Schulte, B. W. Busch, E. Garfunkel, T. Gustafsson, G. Schiwietz, and P. L. Grande, Nucl. Instrum. Methods Phys. Res. B **183**, 16 (2001).
[13] P. L. Grande, A. Hentz, G. Schiwietz, W. H. Schulte, B. W. Busch, D. Starodub, and T. Gustafsson, Phys. Rev. B **69**, 104112 (2004).
[14] P. F. A. Alkemade, W. C. Turkenburg, and J. Vrijmoeth, Nucl. Instrum. Methods Phys. Res. B **64**, 716 (1992).
[15] P. Bailey, T. C. Q. Noakes, and D. P. Woodruff, Surf. Sci. **426**, 358 (1999).
[16] R. M. Tromp, M. Copel, M. C. Reuter, M. Horn von Hoegen, J. Speidell, and R. Koudijs, Rev. Sci. Instrum. **62**, 2679 (1991).
[17] D. Brown, T. C. Q. Noakes, D. P. Woodruff, P. Bailey, and Y. Le Goaziou, J. Phys.: Condens. Matter **11**, 1889 (1999).
[18] R. M. Tromp, M. Copel, M. C. Reuter, M. Horn von Hoegen, J. Speidell, and R. Koudijs, Rev. Sci. Instrum. **62**, 2679 (1991).
[19] J. Kim, W. N. Lennard, C. P. McNorgan, J. Hendriks, I. V. Mitchell, D. Landheer, and J. Gredley, Curr. Appl. Phys. **3**, 75 (2003).
[20] J. W. M. Frenken, R. M. Tromp, and J. F. van der Veen, Nucl. Instrum. Methods Phys. Res. B **17**, 334 (1986).
[21] C. Polop, J. L. Sacedón, and J. A. Martín-Gago, Surf. Sci. **454–456**, 842 (2000).
[22] C. Polop, C. Rogero, J. L. Sacedón, and J. A. Martín-Gago, Surf. Sci. **482–485**, 1337 (2001).
[23] W. Fritsch and C. D. Lin, Phys. Rep. **202**, 1 (1991); J. F. Reading, T. Bronk, A. L. Ford, L. A. Wehrman, and K. A. Hall, J. Phys. B **30**, L189 (1997).
[24] J. Bang and J. M. Hansteen, K. Dan. Vidensk. Selsk. Mat. Fys. Medd. **31**, No. 13 (1959); L. Wilets and S. J. Wallace, Phys. Rev. **169**, 84 (1968); M. R. Flannery and K. J. MacCann, Phys. Rev. A **8**, 2915 (1973).
[25] F. Herman and S. Skillmann, *Atomic Structure Calculations*, (Prentice-Hall, Englewood Cliffs, NJ, 1963).